· Article · Advances in Polar Science
doi: 10.12429/j.advps.2023.0012 March 2024 Vol. 35 No. 1: 123-131

Impact of transparent exopolymer particles on the dynamics of dissolved organic carbon in the Amundsen Sea, Antarctica

HU Ji[1], XUE Siyou[1,2], ZHAO Jun[1], LI Dong[1], ZHANG Haifeng[1], YU Peisong[1], ZHANG Cai[1], YANG Xufeng[1] & PAN Jianming[1*]

[1] Key Laboratory of Marine Ecosystem Dynamics, Second Institute of Oceanography, Ministry of Natural Resources, Hangzhou 310012, China;
[2] College of Ocean and Earth Sciences, Xiamen University, Xiamen 361102, China

Received 27 July 2023; accepted 22 December 2023; published online 30 March 2024

Abstract The Southern Ocean is an important carbon sink pool and plays a critical role in the global carbon cycling. The Amundsen Sea was reported to be highly productive in inshore area in the Southern Ocean. In order to investigate the influence of transparent exopolymer particles (TEP) on the behavior of dissolved organic carbon (DOC) in this region, a comprehensive study was conducted, encompassing both open water areas and highly productive polynyas. It was found that microbial heterotrophic metabolism is the primary process responsible for the production of humic-like fluorescent components in the open ocean. The relationship between apparent oxygen utilization and the two humic-like components can be accurately described by a power-law function, with a conversion rate consistent with that observed globally. The presence of TEP was found to have little impact on this process. Additionally, the study revealed the accumulation of DOC at the sea surface in the Amundsen Sea Polynya, suggesting that TEP may play a critical role in this phenomenon. These findings contribute to a deeper understanding of the dynamics and surface accumulation of DOC in the Amundsen Sea Polynya, and provide valuable insights into the carbon cycle in this region.

Keywords **dissolved organic matter**, **chromophoric dissolved organic matter**, **excitation-emission matrix coupled with parallel factor analysis**, **transparent exopolymer particles**, **Amundsen Sea**, **Antarctica**

Citation: Hu J, Xue S Y, Zhao J, et al. Impact of transparent exopolymer particles on the dynamics of dissolved organic carbon in the Amundsen Sea, Antarctica. Adv Polar Sci, 2024, 35(1): 123-131, doi: 10.12429/j.advps.2023.0012

1 Introduction

The Southern Ocean plays a crucial role in the global carbon cycle (Sallée et al., 2012). Due to climate change, the Southern Ocean has undergone significant changes in its biogeochemistry and ecosystem dynamics. The polynyas surrounding Antarctica exhibit high levels of productivity (Arrigo and van Dijken, 2003) and are considered as important areas for carbon dioxide (CO_2) absorption (Arrigo et al., 2008). The Amundsen Sea Polynya (ASP), located in the inshore area during the austral summer, has been identified as having the highest primary production among the 37 coastal polynyas in the Southern Ocean. This is attributed to the release of iron from melting glaciers (Arrigo and van Dijken, 2003). The presence of this highly productive polynya, resulting from glacial retreat, can significantly impact the marine carbon cycle in the Southern Ocean, affecting the dynamics of both inorganic and organic carbon. Of particular interest in the ASP is the dissolved organic matter (DOM), which plays a crucial role

* Corresponding author, E-mail: jmpan@sio.org.cn

in the carbon cycle of the Southern Ocean. DOM comprises a complex mixture of organic compounds released into the water through various biological processes, including primary production, microbial activity, and the decomposition of organic matter (Hansell and Carlson, 1998). However, our current knowledge and understanding of the dynamics of DOM in the ASP are still limited.

Transparent exopolymer particles (TEP) are gel-like acidic polysaccharides that can be stained with Alcian blue (Alldredge et al., 1993). Phytoplankton is considered the primary source of TEP (Alldredge et al., 1993; Engel et al., 2015; Passow, 2002). TEPs can be classified as DOM and exhibit characteristics such as stickiness, low density, and a high carbon to nitrogen ratio (Passow, 2002). TEPs are composed of polysaccharides and proteins, and they have the ability to aggregate organic particles, including bacteria and phytoplankton. These aggregates can affect the vertical transport of organic matter and its availability to other organisms in the marine food web (Passow, 2002). Previous studies have demonstrated that TEPs promote the aggregation of particulate organic particles, leading to the formation of marine snow and subsequent sinking of organic matter to the seafloor (Mari et al., 2017). This process contributes to the sequestration of CO_2 from the atmosphere and enhances the biological pump in the Southern Ocean. Additionally, TEPs can serve as substrates for bacterial growth, resulting in the production of extracellular enzymes that degrade organic matter. It has been observed that TEPs are resistant to bacterial degradation for several hours to days (Stoderegger and Herndl, 1998), potentially enabling long-term carbon storage in the deep ocean. Therefore, the distribution of TEPs plays a crucial role in the carbon cycle of marine ecosystems. Studies have shown that photo-biological stress, sea ice melting, and turbulence can increase phytoplankton productivity and consequently elevate TEP concentrations in the Antarctic Peninsula area and the Atlantic Sector of the Southern Ocean (Zamanillo et al., 2019). Our previous work has revealed high levels of TEPs during blooms in ASP (Xue et al., 2022). Hence, understanding the impact of TEPs on the dynamics of DOM is essential for comprehending the carbon cycle in this region. To the best of our knowledge, there are currently no such reports in the Amundsen Sea.

In this paper, we raise a scientific assumption that the presence of TEP may facilitate the formation of biologically recalcitrant dissolved organic carbon (DOC) but has little impact on chromophoric dissolved organic matter (CDOM). We present findings on the vertical accumulation of DOC and CDOM in the ASP, Antarctica. CDOM refers to the optically active fraction of DOM, as described by Coble (2007). The concentration of TEP was measured to assess their contribution to the surface buildup of DOC. Additionally, we utilized excitation-emission matrix coupled with parallel factor analysis to gain deeper insights into the fluorescent groups present in CDOM. We are confident that our research will yield crucial insights into the pivotal role of TEP within the intricate marine carbon cycle. By the impact of TEP on the distribution and transformation of organic carbon, our study aims to shed light on the intricate processes that govern carbon cycling in marine ecosystems. Through our comprehensive analysis, we anticipate uncovering useful findings that will contribute to a deeper understanding of the complex interactions between TEP and the global carbon budget, ultimately enhancing our ability to mitigate and adapt to climate change.

2 Methods

2.1 Study area and sample collection

During the austral summer, samples were collected in the Amundsen Sea for the analysis of DOC and CDOM. The sampling was conducted during a cruise from 21 to 30 January, 2020 on the R/V *Xuelong*, which belongs to the Polar Research Institute of China (PRIC) (Figure 1 and Table 1). The temperature and salinity profiles (Figure 2) showed that the warm Circumpolar Deep Water (CDW) intruded into the shelf of the Amundsen Sea, even influencing the water column at a depth of 200 m. This observation is consistent with previous studies that reported the intrusion of CDW through glacially scoured troughs on the seafloor (Jacobs et al., 2012). The three main water masses in the area are the relatively cold Antarctic Winter Water (WW), the warm and salty CDW, and the seasonal Antarctic Surface Water (AASW) (Chen et al., 2019). Based on sea ice concentration data collected during the survey, samples were collected in the ASP and Amundsen Sea Open Water (ASOW).

At each station, measurements of pressure, salinity, and temperature were taken using a SBE 911 plus CTD instrument equipped with a rosette sampler containing 24×10 L Niskin bottles. The concentration of oxygen was determined using Winkler titration (Williams and Jenkinson, 1982). Oxygen saturation was calculated using the measured data and the solubility equations of Garcia and Gordon (1992), along with the coefficients of Benson and Krause (1984). The Apparent Oxygen Utilization (AOU), which represents the consumption of oxygen over a given period, was calculated as the difference between oxygen saturation and the measured oxygen concentration at a specific depth. AOU can serve as an indicator of microbial heterotrophic metabolism. The concentration of chlorophyll *a* (Chl *a*) was measured using a Turner fluorimeter on board and has been reported in another publication (Zhang et al., 2022). TEP samples were collected at the surface and the deep chlorophyll maximum (DCM) at five stations (A4-09, A3-08, and A3-06 in ASOW, and A11-02 and A9-01 in ASP).

2.2 Sample treatment

Samples for DOC and CDOM analysis were filtered using pre-combusted Whatman GF/F filters. The filtrate

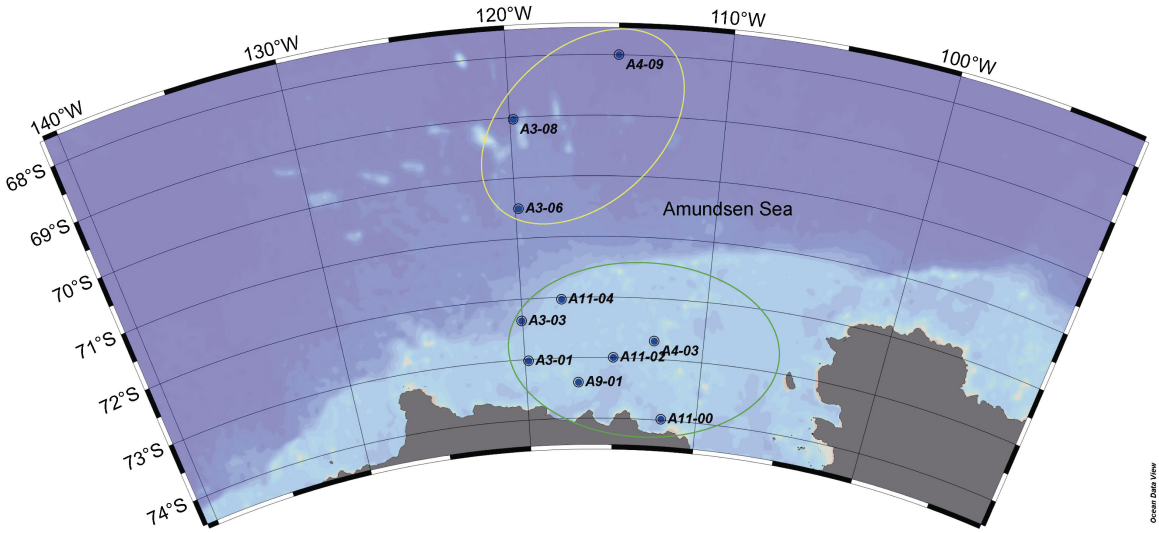

Figure 1 Location of the stations sampled during austral summer in 2020 R/V *Xuelong* cruise. Amundsen Sea Open Water (ASOW) and Amundsen Sea Polynya (ASP) stations were indicated by yellow circles and green circles, respectively.

Table 1 Location details in the study area

Study area	Station	Date/UTC	Longitude	Latitude	Depth/m
ASOW	A3-08	2020-01-21	119.84°W	69.02°S	3600
	A3-06	2020-01-23	119.84°W	70.51°S	2820
	A4-09	2020-01-31	115.00°W	68.00°S	4480
ASP	A11-04	2020-01-25	117.84°W	72.03°S	500
	A11-02	2020-01-26	115.01°W	72.99°S	666
	A11-00	2020-01-27	112.10°W	73.99°S	754
	A4-03	2020-01-27	112.74°W	72.70°S	437
	A9-01	2020-01-29	117.00°W	73.40°S	336
	A3-01	2020-01-29	119.81°W	73.02°S	417
	A3-03	2020-01-30	120.05°W	72.36°S	1755

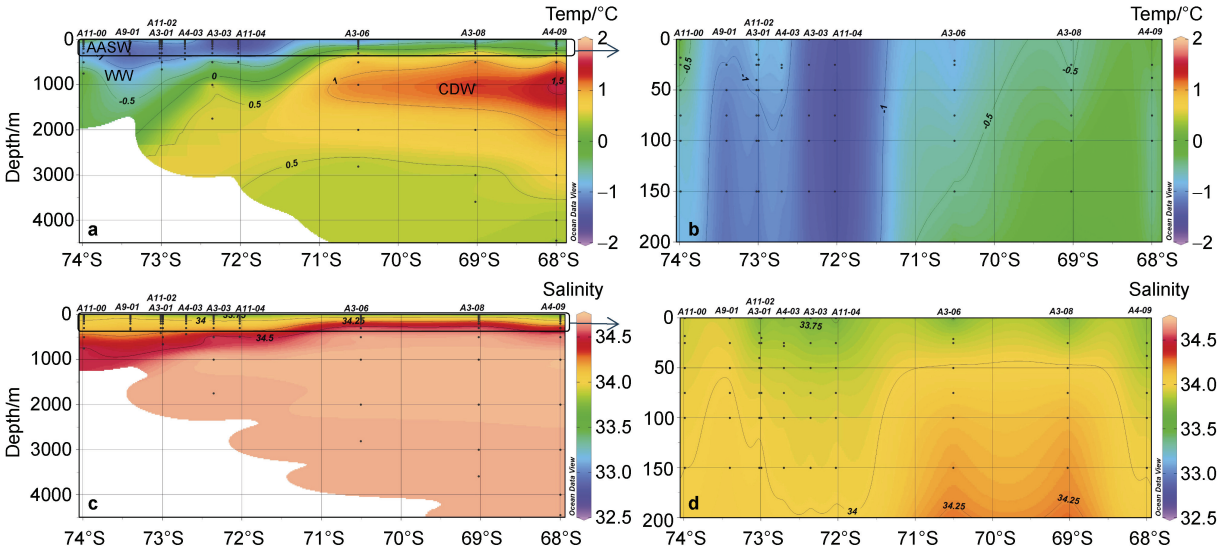

Figure 2 Section profiles of temperature (**a**, from the surface to the bottom; **b**, from the surface to a depth of 200 m) and salinity (**c**, from the surface to the bottom; **d**, from the surface to a depth of 200 m) were examined. The water masses identified in the sections included Winter Water (WW), Circumpolar Deep Water (CDW), and Antarctic Surface Water (AASW).

was then divided into two pre-combusted 20 mL glass ampoules and preserved at −20 ℃ for further analysis in the laboratory on land.

2.3 DOC analysis and estimation of its surface accumulation

The determination of DOC was performed using a Shimadzu TOC-L analyzer employing high temperature combustion. To establish a baseline, Milli-Q water samples (blank) were subtracted, and to ensure measurement accuracy, standard solutions (42–45 μmol·L^{-1} C for the DOC, Deep Sea Reference from University of Miami) were analyzed. The analytical errors, calculated based on replicated measurements (a minimum of three measurements per sample), were found to be within 5% for the DOC.

Surface accumulation of DOC (ΔC_{DOC}) was estimated with the differences in the observed concentrations of DOC between the surface waters and the underlying waters at a depth of 100 m (a depth below the euphotic zone) as used in ASP (Chen et al., 2019) and in the Atlantic Sector of Southern Ocean (Romera-Castillo et al., 2016).

$$\Delta C_{DOC} = C_{DOC,\ surface} - C_{DOC,\ 100m} \quad (1)$$

2.4 CDOM analysis

2.4.1 UV-Vis measurements

CDOM absorbance was measured in the UV and visible spectral range (240–800 nm) using a Shimadzu Spectrophotometer UV-2700 and a 5 cm quartz cuvette with a resolution of 1.0 nm. The absorbance (A) values were converted to Napierian absorption coefficients (a) using Equation (2).

$$a_\lambda = 2.303 \times \frac{A_\lambda}{L} + k\,, \quad (2)$$

where A_λ is the absorbance at the wavelength λ; L is the optical path-length expressed in m; and k is an offset calculated as the mean absorbance between wavelengths 650 nm and 700 nm (approximately zero) (Green and Blough, 1994). The Napierian absorption coefficient (a_λ) was calculated at 325 nm. The reference wavelength of 325 nm was selected to represent the CDOM level (Ortega-Retuerta et al., 2010).

2.4.2 Excitation Emission Matrices

Excitation Emission Matrices (EEMs) were recorded using the Fluorescence Spectrofluorometer (F4700, Hitachi) with a 1×1 cm quartz cuvette. Excitation scans were performed in the range of 250–450 nm, and emission scans were performed in the range of 300–600 nm. The excitation and emission scans had step sizes of 5 nm and 1 nm, respectively. Blank subtraction, instrument correction, and Raman Unit (R.U.) normalization were applied to the EEMs. The EEMs were corrected for instrumental bias and subtracted by the EEM of Milli-Q water measured under the same conditions. The Rayleigh and Raman scatter peaks were removed using three-dimensional interpolation (Zepp et al., 2004). The EEMs were normalized to the water Raman signal (Lawaetz and Stedmon, 2009), and the fluorescence intensity was reported as equivalent water R.U. The EEMs data were analyzed using parallel factor analysis (PARAFAC) with the DOMFluor toolbox (Stedmon and Bro, 2008). The model was validated through visual inspection of the residuals and split half analysis.

2.5 Analysis of TEP concentration

TEP was analyzed according to the experimental method of Passow and Alldredge (1995). A seawater sample of 500 mL was collected, and then filtered through a 25-mm diameter polycarbonate filter membrane with a pore size of 0.45 μm, under conditions of less than 0.02 MPa vacuum. Five hundred μL of Alcian blue with a mass fraction of 0.02% (8GX, pH=2.5, Sigma) were added and left for 2 s until the membrane surface was completely submerged. After washing off the excess dye solution with deionized water, each membrane sample was dissolved in 6 mL 80% sulfuric acid and left for 2 h. During this time the test tube was shaken manually 3–5 times. Finally, the supernatant was taken up into a 1-cm cuvette, and the absorbance was measured at a wavelength of 787 nm. Triplicate samples were collected for each layer. The final results were recorded after deducting the filter blank. The absorbance was calculated by the modified xanthan gum calibration method (Bittar et al., 2018). The surface accumulation of TEP (ΔC_{TEP}) is calculated by the difference of TEP concentration at surface and DCM. The positive and negative values of ΔC_{TEP} indicate upward flux and downward flux of TEP, respectively.

2.6 Statistics

The data plot was generated using Ocean Data View (Schlitzer, 2019) and Origin 9.65 software. To evaluate the differences in response between two categories, a two-sample t-test was conducted, employing a p-value threshold of 0.05 or 0.01 to establish statistical significance.

3 Results

3.1 Spacial distributions of Chl *a* and TEP

During the survey, phytoplankton blooms were observed in the upper layers of the ASP, as indicated by the data on Chl *a,* DO and AOU (Figure 3). Conversely, low concentrations of Chl *a* were found in the ASOW. The mean Chl *a* concentration in ASP was 3.06 mg·L^{-1}, while in ASOW it was 0.25 mg·L^{-1} (Table 2). The vertical integrated Chl *a* concentrations within ASP (0–200 m) were significantly higher than those within ASOW, and these high concentrations were associated with shallow mixed-layer depths and near-shelf regions (Zhang et al., 2022). Furthermore, compared to stations in ASOW, ASP

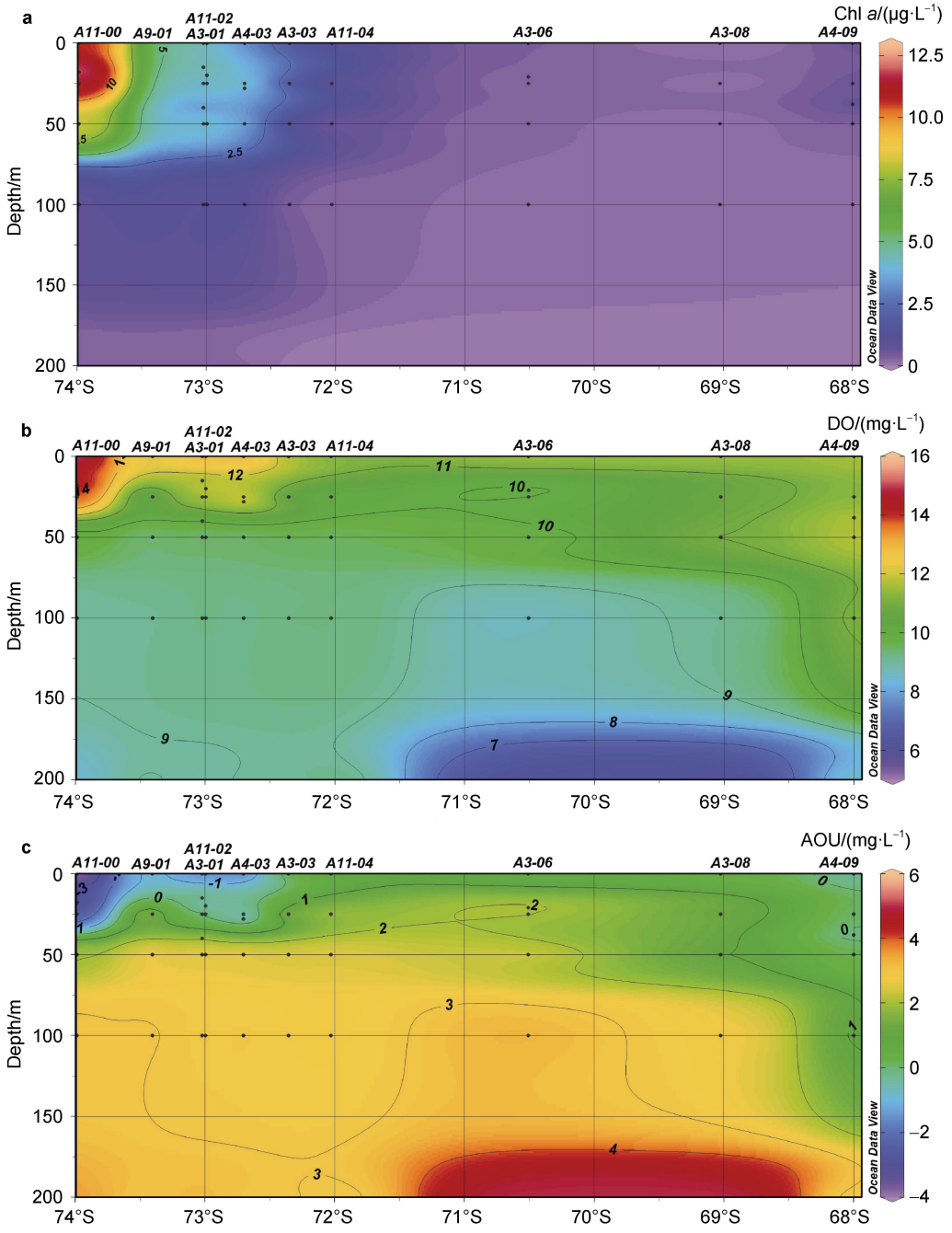

Figure 3 Profiles of Chl *a* (**a**), DO (**b**), and AOU (**c**) in the Amundsen Sea. The data of Chl *a* concentrations in our paper is from partial work of Zhang (2022).

Table 2 Mean values and ranges (minimum and maximum) of environmental variables within 200 m in the study area

Area	Temperature/℃	Salilnity	Chl a^{*}/(mg·L^{-1})	DO**/(mg·L^{-1})	DOC**/(mg·L^{-1})	AOU**/(mg·L^{-1})	a_{325}/(m^{-1})	TEP/(mg Xeq.·L^{-1})
ASOW	−0.50	33.90	0.25	10.02	0.59	1.72	0.31	9.91
	(−1.63–1.72)	(32.68–34.62)	(nd–0.74)	(5.95–11.79)	(0.46–0.89)	(−0.31–5.06)	(0.14–0.58)	(2.07–21.93)
ASP	−0.82	33.86	3.06	10.53	0.55	1.31	1.18	48.46
	(−1.78–1.55)	(32.83–34.14)	(0.02–12.27)	(8.48–15.12)	(0.35–1.58)	(−3.97–3.51)	(nd–6.32)	(3.01–75.48)

Notes: * means the data of Chl *a* concentrations in our paper is from partial work of Zhang (2022); ** means unpublished data; nd means no detection.

exhibited high levels of surface TEP and ΔC_{TEP} (Figure 4a). The mean TEP concentration in ASP was 48.46 mg·L^{-1}, while it was 9.91 mg·L^{-1} in ASOW (Table 2). These findings indicate a high productivity in the upper layer of ASP during the survey.

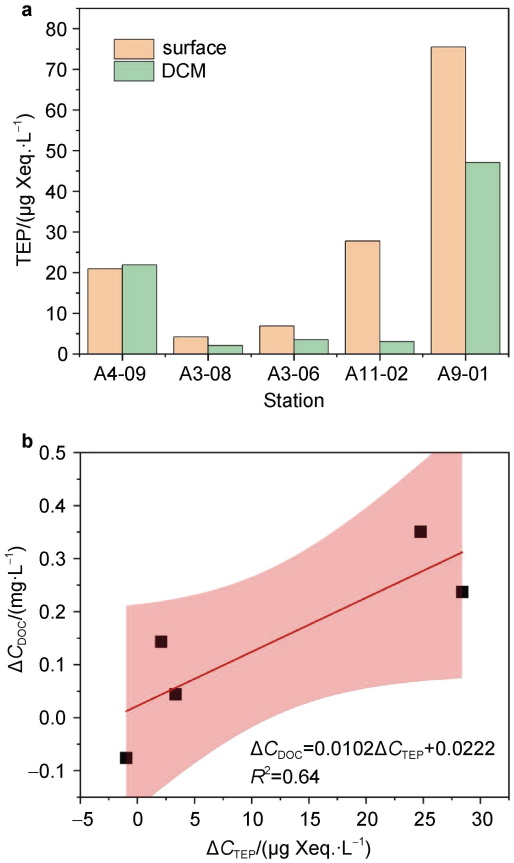

Figure 4 Distribution of TEP at surface and DCM (**a**) and linear relationships between ΔC_{DOC} and ΔC_{TEP} (**b**). The red line in **b** is the linear regression fitting (n=5) and the pink shaded areas represent 95% confidence.

3.2 Surface accumulation of DOC and CDOM

Figure 5 displays the accumulation of DOC and CDOM in ASP. Positive and relatively high accumulations of DOC were observed at the surface water of most stations in ASP (except for A11-04, a station located at the edge of the polynya). The maximum ΔC_{DOC} value of 0.35 mg·L^{-1} was recorded at the center of ASP (station A11-02). In contrast, the surface accumulations of CDOM, indicated by Δa_{325}, showed positive but relatively low values ranging from 0.23 to 0.76 m^{-1}. The highest Δa_{325} value of 4.10 m^{-1} was found at a depth of 25 m in ASP.

3.3 PARAFAC components

In this study, the PARAFAC method was employed, and two groups of humic-like fluorophores were identified in the dataset. Component 1 (C1) exhibited a primary excitation wavelength (Ex) of 255 nm and an emission wavelength (Em) of 444 nm. A secondary Ex peak with lower intensity was observed at 355 nm. C1 displayed spectral characteristics similar to the humic-like component (peak A+C) described by Coble et al. (1998). Component 4 (C4) had a primary and secondary excitation peak, occurring around 250 nm or less and 310 nm, respectively, with a single emission peak at 372 nm. This component exhibited absorption of UVC and UVB light and resembled a marine humic-like component (peak M) found at Em 370–420 nm and Ex 290–310 nm (Coble, 1996).

4 Discussion

4.1 TEP impact on the distribution of humic-like components

Previous studies have shown that marine phytoplankton is the primary source of CDOM. However, the relationship between CDOM and phytoplankton is indirect, with bacteria playing a crucial role in CDOM production (Cammack et al., 2004). Generalized additive models can be used to investigate the main environmental factors influencing fluorescent components in the global ocean (Catalá et al., 2016). It was found that AOU has the greatest impact on the global distribution of humic-like components, followed by Chl *a*, with a power-law relationship. Power-law regression analysis revealed that AOU in the ASOW accounted for 61% of the variation in C1 and 41% in C4, confirming that microbial heterotrophic metabolism is the primary process for humic-like component production in this region (Figure 6 and Table 3). Rochelle-Newall and Fisher (2002) proposed that bacteria can produce humic fluorescence through the release of non-fluorescent organic matter by phytoplankton. Numerous studies have reported a strong correlation between the production of aquatic humic-like fluorophores and microbial activity (Stedmon and Markager, 2005). Additionally, the exponential parameter (b) values for C1 and C4 in the epipelagic layer of ASOW, obtained from power-law regression analysis, were approximately equal (0.24±0.04 for C1 and 0.23±0.07 for C4), and consistent with the mean values for the global ocean's epipelagic layer (0.25±0.02 for C1 and 0.26±0.02 for C4) (Catalá et al., 2016). However, these values were lower than the mean values for the global deep ocean (0.51±0.04 for C1 and 0.31±0.04 for C4) (Catalá et al., 2015). This indicates that the conversion rate of humic components by bacteria in the presence of TEP in the study area is consistent with that of the global ocean's epipelagic layer, but lower than that of the global deep sea. The results suggest that TEP has little impact on the distribution of humic-like components of CDOM.

4.2 Influence of TEP on the surface accumulation of DOC in ASP

Based on the ΔC_{DOC} profile of the Amundsen Sea

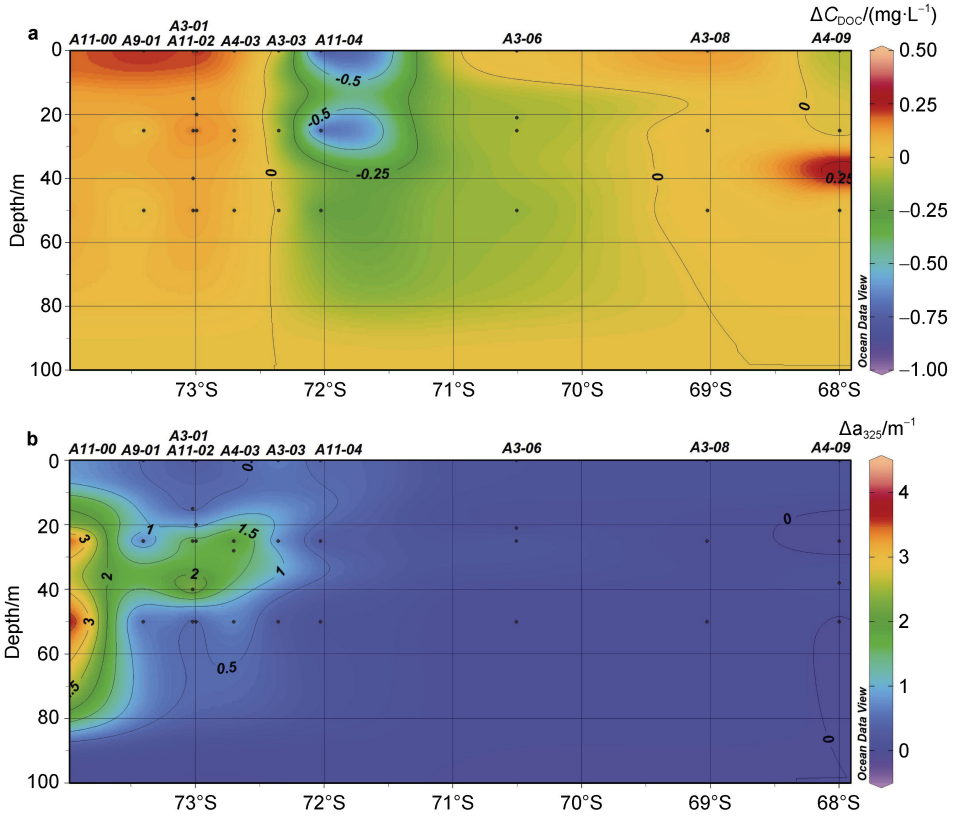

Figure 5 The accumulation of DOC (**a**) and CDOM (**b**) at the ocean surface of the Amundsen Sea.

Table 3 The results of power-law regression fitting in each area and comparisons with those in global epipelagic ocean and dark global ocean

Area	C1				C4				Source
	a/(×10^{-3})	b	R^2	p	a/(×10^{-3})	b	R^2	p	
ASOW	11.59±0.56	0.24±0.04	0.61	<0.0001	5.77±0.41	0.23±0.07	0.41	<0.0001	This work
ASP	13.42±1.07	0.14±0.08	0.08	<0.0001	6.65±0.75	0.20±0.11	0.08	<0.0001	This work
Global epipelagic ocean	3.0±0.3	0.25±0.02	0.73	<0.0001	2.9±0.2	0.26±0.02	0.80	<0.0001	Catalá et al., 2016
Dark global ocean	0.09±0.02	0.51±0.04	0.9	<0.001	2.0±0.4	0.31±0.04	0.79	<0.001	Catalá et al., 2015

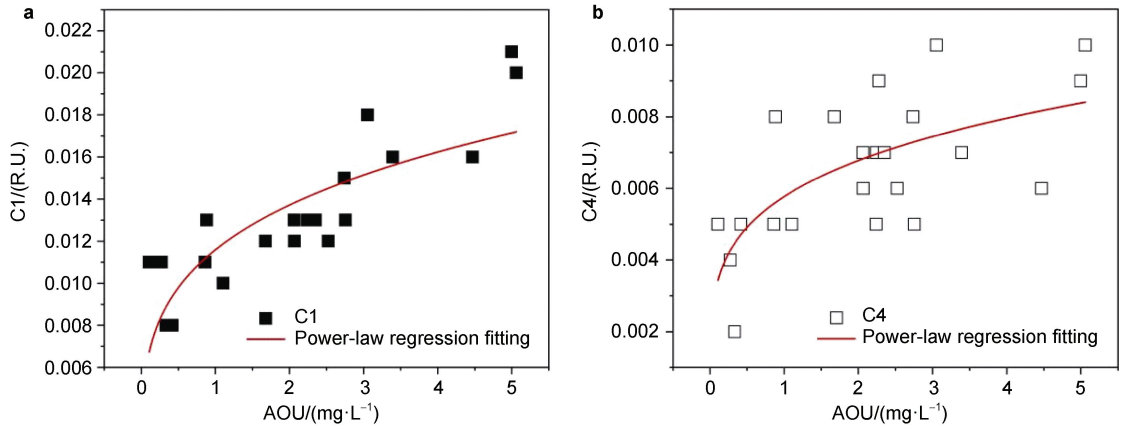

Figure 6 Relationships between the humic-like fluorescence PARAFAC components C1 (**a**) and C4 (**b**) and AOU in ASOW. The power-law function used for fitting is $C(n)$=a·(AOU)^b. Note: AOU values lower than 0 were not considered in the AOU-components relationships.

section (Figure 5a), positive surface accumulation of DOC was observed at most stations in the ASP, with the exception of station A11-04 located at the polynya edge. This station may experience dilution and influence from ice-melting water, resulting in reduced surface DOC levels. The highest surface accumulation of DOC was found at the center of ASP, with a ΔC_{DOC} value of 0.35 mg·L^{-1} (station A11-02). To assess the efficiency of vertical export of DOC from surface water to the deep zone, net DOC production ratios (NDPr) were calculated. NDPr values for ASP (9%±6%) and the value of Ross Sea (as low as 4%) were lower than the global trend (17%) (Hansell and Carlson, 1998), indicating lower surface accumulation and export efficiency in these regions. Several scenarios were proposed to explain the low surface accumulation of DOC in ASP, including a eutrophic ecosystem and the labile nature of freshly produced DOM in the surface layer. The Δa_{325} profile of the Amundsen Sea section (Figure 5b) showed a positive but low accumulation of CDOM in the surface water. This differs from previous findings of negative accumulation in ASP, which may be attributed to variations in solar radiation levels among different investigations. The location of the maximum a_{325} value beneath the surface water suggests a photo-labile nature of CDOM. Additionally, the foam-like structure of the predominant phytoplankton taxon *Phaeocystis antarctica* was hypothesized to contribute to the prolonged residence time of DOC in the Amundsen Sea (Chen et al., 2019).

In the euphotic layer of the Amundsen Sea, the presence of TEP has the potential to significantly contribute to the accumulation of DOC at the surface. Our analysis shows a strong positive correlation between ΔC_{TEP} and ΔC_{DOC} ($p < 0.001$) (Figure 4b). In fact, the variation in ΔC_{TEP} can explain up to 64% of the variation in ΔC_{DOC} indicating that the upward flux of TEP plays a major role in the surface accumulation of DOC.

TEP is characterized by a high carbon/nitrogen (C/N) ratio and has been found to have a mean C/N ratio of 26 in incubated marine algae (Engel and Passow, 2001). Although the exact carbon content of TEP is still difficult to be determined accurately, a conversion factor of TEP concentration (mg Xeq.·L^{-1}) to TEP-C (mg C·L^{-1}) has been globally applied, ranging from 0.51 to 0.88 (Engel and Passow, 2001), based on the dominant species of phytoplankton in the ocean. Even using the highest conversion factor of 0.88, the estimated TEP-C only accounts for a minor portion, up to 28%, of the accumulated DOC. This suggests that the carbon in TEP itself was not the majority of accumulated DOC.

The net accumulation of DOC in the open ocean is primarily driven by the decoupling of biological production and consumption processes (Hansell, 2002). Labile DOC, which is freshly produced, can be adsorbed onto colloids and transformed into a form that is too complex for enzymatic degradation. This abiotic formation of biologically recalcitrant DOC has been proposed as a potential mechanism (Nagata and Kirchman, 1996).

In this study, we propose a hypothesis that the phytoplankton bloom in ASP releases an amount of TEP and TEP precursors. Due to the limited input of dense material from surrounding land runoff in this area, gel-like TEP and precursors can abiotically form aggregates with low density relative to seawater, resulting in a longer residence time in the upper water column. These TEP aggregates have the ability to adsorb labile DOC and transform it into a biologically recalcitrant form, leading to the accumulation of DOC in the surface water. Additionally, the prolonged residence of DOC in the upper layer, facilitated by these aggregates, increases its exposure to solar radiation, promoting the decomposition of CDOM. This may ultimately result in a less positive or even negative accumulation of CDOM in the surface water.

5 Conclusion

The ASP, during the austral summer of 2020, exhibited a significant phytoplankton bloom in the upper water column. This bloom led to the production of TEP, which have the ability to convert labile DOC into a biologically recalcitrant form in the surface water. Consequently, TEP may play a crucial role in the accumulation of DOC in the high productivity ASP.

To fully comprehend the role of TEP in DOM accumulation and its impact on the carbon cycle in this region, further research is required. Field studies, laboratory experiments, and modeling studies can all contribute to our understanding of TEP production, composition, and their effects on the aggregation and transport of organic matter. By investigating the factors influencing TEP concentration and composition, as well as their relationship with environmental variables, we can enhance our ability to predict future changes in the carbon balance within the Southern Ocean.

Acknowledgments The authors thank the Polar Research Institute of China and the crew of R/V *Xuelong* for their assistance in sample collection and analysis on board. This research was funded by the National Natural Science Foundation of China (Grant nos. 42276255 and 41976227), and project "Impact and Response of Antarctic Seas to Climate Change, IRASCC 2020-2022" (Grant nos. 01-01-02A and 02-02-05). We appreciate two anonymous reviewers and Associate Editor Dr. Liyang Zhan for constructive comments that helped us improve the manuscript.

References

Alldredge A L, Passow U, Logan B E. 1993. The abundance and significance of a class of large, transparent organic particles in the ocean. Deep Sea Res Part I Oceanogr Res Pap, 40(6): 1131-1140, doi:10.1016/0967-0637(93)90129-q.

Arrigo K R, van Dijken G L. 2003. Phytoplankton dynamics within 37 Antarctic coastal polynya systems. J Geophys Res, 108(C8): 3271, doi: 10.1029/2002jc001739.

Arrigo K R, van Dijken G, Long M. 2008. Coastal Southern Ocean: a strong anthropogenic CO_2 sink. Geophys Res Lett, 35(21): L21602, doi:10.1029/2008gl035624.

Benson B B, Krause D Jr. 1984. The concentration and isotopic fractionation of oxygen dissolved in freshwater and seawater in equilibrium with the atmosphere. Limnol Oceanogr, 29(3): 620-632, doi:10.4319/lo.1984.29.3.0620.

Bittar T B, Passow U, Hamaraty L, et al. 2018. An updated method for the calibration of transparent exopolymer particle measurements. Limnol Oceanogr Meth, 16(10): 621-628, doi:10.1002/lom3.10268.

Cammack W K L, Kalff J, Prairie Y T, et al. 2004. Fluorescent dissolved organic matter in lakes: relationships with heterotrophic metabolism. Limnol Oceanogr, 49(6): 2034-2045, doi:10.4319/lo.2004.49.6.2034.

Catalá T S, Reche I, Fuentes-Lema A, et al. 2015. Turnover time of fluorescent dissolved organic matter in the dark global ocean. Nat Commun, 6: 5986, doi:10.1038/ncomms6986.

Catalá T S, Álvarez-Salgado X A, Otero J, et al. 2016. Drivers of fluorescent dissolved organic matter in the global epipelagic ocean. Limnol Oceanogr, 61(3): 1101-1119, doi:10.1002/lno.10281.

Chen M, Jung J, Lee Y K, et al. 2019. Production of tyrosine-like fluorescence and labile chromophoric dissolved organic matter (DOM) and low surface accumulation of low molecular weight-dominated DOM in a productive Antarctic sea. Mar Chem, 213: 40-48, doi:10.1016/j.marchem.2019.04.009.

Coble P G. 1996. Characterization of marine and terrestrial DOM in seawater using excitation-emission matrix spectroscopy. Mar Chem, 51(4): 325-346, doi:10.1016/0304-4203(95)00062-3.

Coble P G. 2007. Marine optical biogeochemistry: the chemistry of ocean color. Chem Rev, 107(2): 402-418, doi:10.1021/cr050350+.

Coble P G, Del Castillo C E, Avril B. 1998. Distribution and optical properties of CDOM in the Arabian Sea during the 1995 Southwest Monsoon. Deep Sea Res Part II Top Stud Oceanogr, 45(10/11): 2195-2223, doi:10.1016/s0967-0645(98)00068-x.

Engel A, Passow U. 2001. Carbon and nitrogen content of transparent exopolymer particles (TEP) in relation to their Alcian Blue adsorption. Mar Ecol Prog Ser, 219: 1-10, doi:10.3354/meps219001.

Engel A, Borchard C, Loginova A, et al. 2015. Effects of varied nitrate and phosphate supply on polysaccharidic and proteinaceous gel particle production during tropical phytoplankton bloom experiments. Biogeosciences, 12(19): 5647-5665, doi:10.5194/bg-12-5647-2015.

Garcia H E, Gordon L I. 1992. Oxygen solubility in seawater: better fitting equations. Limnol Oceanogr, 37(6): 1307-1312, doi:10.4319/lo.1992.37.6.1307.

Green S A, Blough N V. 1994. Optical absorption and fluorescence properties of chromophoric dissolved organic matter in natural waters. Limnol Oceanogr, 39(8): 1903-1916, doi:10.4319/lo.1994.39.8.1903.

Hansell D A. 2002. Chapter 15–DOC in the global ocean carbon cycle//Hansell D A, Carlson C A (eds). Biogeochemestry of marine dissolved organic matter, 1st edition, San Diego: Academic Press, 685-714, doi:10.1016/B978-012323841-2/50017-8.

Hansell D A, Carlson C A. 1998. Net community production of dissolved organic carbon. Glob Biogeochem Cycles, 12(3): 443-453, doi:10.1029/98gb01928.

Jacobs S, Jenkins A, Hellmer H, et al. 2012. The Amundsen Sea and the Antarctic Ice Sheet. Oceanogr, 25(3): 154-163, doi:10.5670/oceanog.2012.90.

Lawaetz A J, Stedmon C A. 2009. Fluorescence intensity calibration using the Raman scatter peak of water. Appl Spectrosc, 63(8): 936-940, doi:10.1366/000370209788964548.

Mari X, Passow U, Migon C, et al. 2017. Transparent exopolymer particles: effects on carbon cycling in the ocean. Prog Oceanogr, 151: 13-37, doi:10.1016/j.pocean.2016.11.002.

Nagata T, Kirchman D L. 1996. Bacterial degradation of protein adsorbed to model submicron particles in seawater. Mar Ecol Prog Ser, 132(1-3): 241-248, doi:10.3354/meps132241.

Ortega-Retuerta E, Reche I, Pulido-Villena E, et al. 2010. Distribution and photoreactivity of chromophoric dissolved organic matter in the Antarctic Peninsula (Southern Ocean). Mar Chem, 118(3/4): 129-139, doi:10.1016/j.marchem.2009.11.008.

Passow U. 2002. Transparent exopolymer particles (TEP) in aquatic environments. Progr Oceanogr, 55(3/4): 287-333, doi:10.1016/S0079-6611(02)00138-6.

Passow U, Alldredge A L. 1995. Aggregation of a diatom bloom in a mesocosm: the role of transparent exopolymer particles (TEP). Deep Sea Res Part II Top Stud Oceanogr, 42(1): 99-109, doi:10.1016/0967-0645(95)00006-c.

Rochelle-Newall E J, Fisher T R. 2002. Production of chromophoric dissolved organic matter fluorescence in marine and estuarine environments: an investigation into the role of phytoplankton. Mar Chem, 77(1): 7-21, doi:10.1016/S0304-4203(01)00072-X.

Romera-Castillo C, Letscher R T, Hansell D A. 2016. New nutrients exert fundamental control on dissolved organic carbon accumulation in the surface Atlantic Ocean. Proc Natl Acad Sci USA, 113(38): 10497-10502, doi:10.1073/pnas.1605344113.

Sallée J B, Matear R J, Rintoul S R, et al. 2012. Localized subduction of anthropogenic carbon dioxide in the Southern Hemisphere oceans. Nat Geosci, 5(8): 579-584, doi:10.1038/ngeo1523.

Schlitzer R. 2019. Ocean Data View. http://odv.awi.de.

Stedmon C A, Bro R. 2008. Characterizing dissolved organic matter fluorescence with parallel factor analysis: a tutorial. Limnol Oceanogr: Methods, 6(11): 572-579, doi:10.4319/lom.2008.6.572.

Stedmon C A, Markager S. 2005. Tracing the production and degradation of autochthonous fractions of dissolved organic matter by fluorescence analysis. Limnol Oceanogr, 50: 1415-1426.

Stoderegger K, Herndl G J. 1998. Production and release of bacterial capsular material and its subsequent utilization by marine bacterioplankton. Limnol Oceanogr, 43(5): 877-884, doi:10.4319/lo.1998.43.5.0877.

Williams P J, Jenkinson N W. 1982. A transportable microprocessor-controlled precise Winkler titration suitable for field station and shipboard use. Limnol Oceanogr, 27(3): 576-584, doi:10.4319/lo.1982.27.3.0576.

Xue S Y, Hu J, Feng Y B, et al. 2022. Distribution of transparent exopolymer particles and their response to phytoplankton community structure changes in the Amundsen Sea, Antarctica. Adv Polar Sci, 33(1): 44-54, doi: 10.13679/j.advps.2021.0034.

Zamanillo M, Ortega-Retuerta E, Nunes S, et al. 2019. Main drivers of transparent exopolymer particle distribution across the surface Atlantic Ocean. Biogeosciences, 16(3): 733-749, doi:10.5194/bg-16-733-2019.

Zepp R G, Sheldon W M, Moran M A. 2004. Dissolved organic fluorophores in southeastern US coastal waters: correction method for eliminating Rayleigh and Raman scattering peaks in excitation-emission matrices. Mar Chem, 89(1-4): 15-36, doi:10.1016/j.marchem.2004.02.006.

Zhang W, Hao Q, He J F, et al. 2022. Variability of size-fractionated phytoplankton in the Amundsen Sea during summer. Adv Polar Sci, 33(1): 1-13, doi:10.13679/j.advps.2021.0035.